Shape Changes of Pt Nanoparticles Induced by Deposition on Mesoporous Silica

Lisandro J. Giovanetti, José M. Ramallo-López, Michael Foxe, Louis C. Jones, Matthias M. Koebel, Gabor A. Somorjai, Aldo F. Craievich, Miquel B. Salmeron, and Félix G. Requejo*

***P**olyvinylpyrollidone (PVP)-capped platinum nanoparticles (NPs) are found to change shape from spherical to flat when deposited on mesoporous silica substrates (SBA-15). Transmission electron microscopy (TEM), small-angle X-ray scattering (SAXS), and extended X-ray absorption fine structure (EXAFS) analyses are used in these studies. The SAXS results indicate that, after deposition, the 2 nm NPs have an average gyration radius 22% larger than in solution, while the EXAFS measurements indicate a decrease in first neighbor co-ordination number from 9.3 to 7.4. The deformation of these small capped NPs is attributed to interactions with the surface of the SBA-15 support, as evidenced by X-ray absorption near-edge structure (XANES).*

1. Introduction

It has been proposed that the reaction rate, activity, and selectivity of many reactions on nanoparticle (NP) catalysts depend on their morphology, size,[1] crystal structure,[2] and composition.[3–5] While traditional methods to synthesise particles typically lead to a broad size distributions and random shape distributions, novel methods based on colloidal syntheses have been developed that enable precise control of shape and size,[6] thus allowing for studies to determine the correlation between chemical and structural properties.[7,8] It has been demonstrated that the structure of supported NPs depends on the nature of the substrate.[9–12] The interaction between the nanoparticle and the support surface induces changes in the wetting of the metal on the support surface. This type of change produces deformation in the nanoparticle shape and depends strongly on the chemical properties of the support.[13,14]

Here we report the results of investigations of the changes in the shape of Pt NPs capped with polyvinylpyrollidone (PVP). Specifically, the initial ≈2 nm spherical particles are observed to change shape after deposition onto SBA-15 porous silica substrates. Our study was performed using several techniques, including transmission electron microscopy (TEM), small-angle X-ray scattering (SAXS) and extended X-ray absorption fine structure (EXAFS). We found that the SBA-supported NPs flatten out relative to the same particles before impregnation, a result that demonstrates the importance of particle–substrate interaction for small NPs, even without removal of the PVP capping. The change in shape of the SBA-supported NPs may have important implications in understanding the catalytic properties of supported nanoparticles.

Dr. L. J. Giovanetti, Dr. J. M. Ramallo-López, Prof. F. G. Requejo
Instituto de Investigaciones Fisicoquıímicas
Teóricas y Aplicadas (INIFTA)
FCE, Universidad Nacional de La Plata - CONICET
Sucursal 4 Casilla de Correo 16 (1900), La Plata, Argentina
E-mail: lisandro@fisica.unlp.edu.ar
Dr. M. Foxe, Dr. L. C. Jones, Prof. G. A. Somorjai, Prof. M. B. Salmeron
Materials Science Division
Lawrence Berkeley National Laboratory
Berkeley, CA 94720, USA
Dr. M. M. Koebel
Swiss Federal Laboratories for Materials Science and Technology
Empa, CH-8600 Dübendorf, Switzerland
Prof. A. F. Craievich
Institute of Physics. University of Sao Paulo
CEP 05508-900 Sao Paulo, Brazil

DOI: 10.1002/smll.201101293

small NANO MICRO

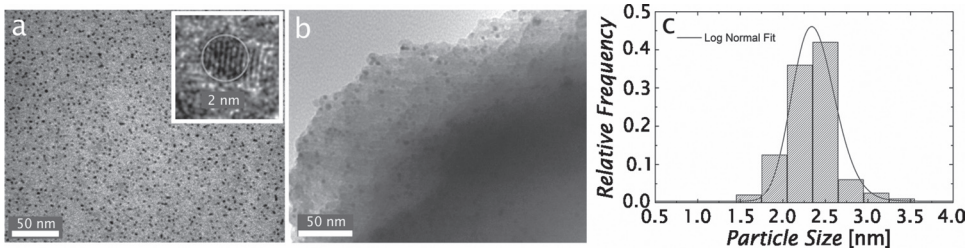

Figure 1. a) TEM image of PVP-capped Pt NPs showing a narrow dispersion of sizes. The inset shows a NP with clearly visible crystallographic lattice planes. b) TEM image of a SBA-15 substrate after being impregnated with capped Pt NPs. c) Particle size distribution of capped Pt NPs before impregnation with a corresponding Log–normal fit.

2. Results and Discussion

2.1. Transmission Electron Microscopy (TEM)

PVP-capped Pt NPs dispersed in a colloidal suspension were deposited on a carbon film membrane and analyzed by TEM. An example of the images obtained is shown in **Figure 1**a. To characterize their size and shape the average long and short diameters (D_{max} and D_{min} respectively) of the NPs were measured from the images. On average, the asymmetry factor (D_{max}/D_{min}) is lower than 1.07, which indicates that the NPs are nearly spherical. The size distribution is quite narrow with an average radius $<R>$ = 1.18 nm and a standard deviation σ = 0.12 nm. A histogram is shown in Figure 1c.

The inset in Figure 1a displays a small area of the same image with a higher magnification. The (111) crystallographic planes of this particular NP is perpendicular to the image and are spaced by 0.21 ± 0.03 nm, which is in good agreement with the 0.226 nm value of bulk Pt. A TEM image of NPs after impregnation on SBA-15 is shown in Figure 1b. The contrast of the picture however is not sufficient for a clear determination of their shape. This will be analyzed with X-ray techniques and discussed in the following sections.

2.2. Small-Angle X-ray Scattering (SAXS)

2.2.1. Guinier Equation

PVP-capped Pt NPs in a diluted ethanol suspension and a powdered porous SBA-15 substrate impregnated with the same Pt NPs were studied by SAXS in transmission mode at room temperature. In order to determine the shape and size of the Pt NPs we analyzed the results with an isotropic two electron-density model assuming that the particles are spatially uncorrelated. Under these assumptions the Guinier equation holds in the limit of low scattering vector (q) values and is written as[15]

$$I(q) = N(\Delta\rho_{pm})^2 < v^2 > e^{-\frac{1}{3}<R_g>_G^2 q^2} \quad (1)$$

where $I(q)$ is the SAXS intensity as a function of q, N is the number of NPs per unit volume, $\Delta\rho_{pm}$ is the difference in electron density between the NP and the liquid matrix; $<v^2>$ the NP average squared volume and $<R_g>_G$ is the Guinier average of the NP gyration radius. The maximum q value for which the Guinier equation holds depends on the shape, size, and distribution of the NP, as discussed in the Supporting Information (SI).

2.2.2. Pt NPs in Liquid Suspension

We assume that the SAXS intensity produced by the NPs in the liquid suspension is essentially due to the Pt core, which is a good approximation given the large difference in electron density between the capping polymer or ethanol, and the Pt core. The SAXS intensity from a colloidal suspension of PVP-capped NPs in ethanol is shown in **Figure 2**a (upper). The same data is displayed as a Guinier plot (log $I(q)$ versus q^2) in Figure 2b (lower). The curve in Figure 2b exhibits a linear behavior in the 1.4 nm^{-2} < q^2 < 6.7 nm^{-2} range with a positive deviation below 1.4 nm^{-2}, which is probably due to incipient NP aggregation. The wide range over which a linear behavior is observed indicates that most of the NPs are not aggregated and corresponds to the main mode of the size distribution function.

The Guinier average of the radius of gyration is usually determined from the slope α of the straight line through the relation $\langle R_g \rangle_G$ (nm) = $2.63\sqrt{\alpha(\text{nm}^{-2})}$. Our results for the NP in colloidal suspension (Figure 2a, bottom) yield a value of $<R_g>_G$ = 0.81 ± 0.01 nm. Hence, the Guinier average of the radius R (assuming a spherical shape) is $<R>_G$ = 1.05 ± 0.01 nm.

A different model of the SAXS intensity that assumes a dilute set of spherical NP with a Gaussian radius distribution is reported in the SI. This allowed us to determine the average radius of the Pt NPs, $<R>$ = 0.89 nm, with standard deviation σ = 0.14 nm. Taking into account that the Guinier average weighs more for larger NPs, the result of this modeling is consistent with that previously derived from the Guinier plot, $<R>_G$ = 1.05 nm. The average radius $<R>$ = 0.89 nm derived from SAXS results is 20% lower than that derived from TEM, $<R_{TEM}>$ = 1.18 nm. The reason for the higher value in the TEM analysis is probably related to the fact that the smaller NP (R < 0.5 nm) are more difficult to detect in the TEM images.

2.2.3. Pt Nanoparticles Supported on an SBA-15 Substrate

Capped Pt NPs were impregnated on a powdered SBA-15 substrate. SBA-15 is a porous material consisting of an ordered arrangement of cylindrical nanopores hexagonally

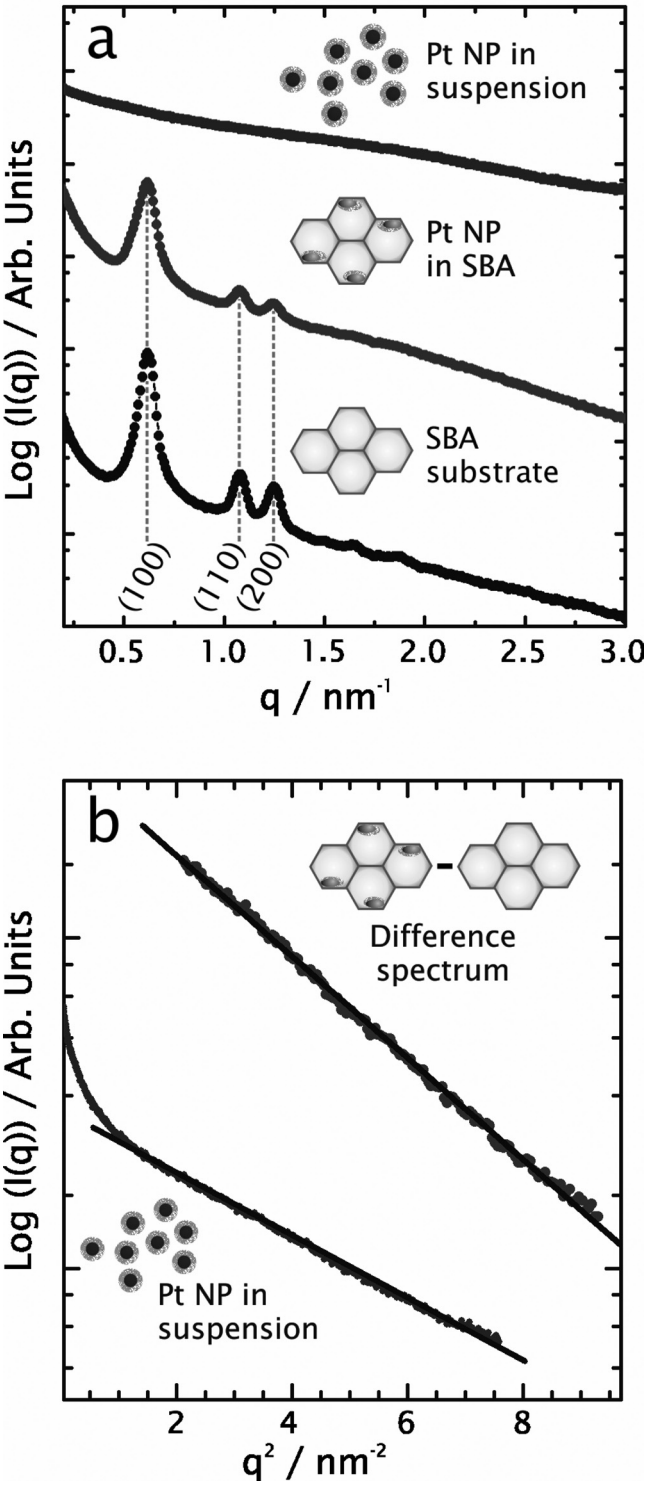

Figure 2. a) Experimental SAXS curves obtained for PVP-capped Pt NPs in dilute ethanol colloidal suspension (upper), embedded in SBA-15 (middle), and the same SBA-15 powder before impregnation (lower). b) Guinier plots (log $I(q)$ versus $q2$) for NPs in an ethanol suspension (bottom) and the difference between the SAXS curves of the impregnated and not impregnated SBA-15 samples (top). The solid straight line corresponds to the Gaussian function of the Guinier equation that best fits the experimental data. The curves are vertically offset for clarity.

packed.[16] As shown in Figure 2a, middle and lower curves, the peaks corresponding to the (100), (110), and (200) Bragg reflections are located at the same q values for samples before and after NP impregnation, indicating that the structure of the SBA-15 substrate was not changed by the impregnation.

The SAXS intensity due to the NPs can be obtained from the difference between the intensity curves before and after impregnation. This assumes that the positions of the NPs and the SBA-15 pores are uncorrelated (or weakly correlated). Details about the subtraction procedure are reported in the SI. The difference is displayed in the top of Figure 2b. The Guinier plot of the difference curve exhibits a linear behavior over a wide q range, indicating that the NPs are dispersed in the SBA-15 substrate and that the interaction between the NPs and the SBA-15 pore surfaces is enough to prevent clustering. From the slope of the straight line in Figure 2b (top) the Guinier average of the radius of gyration of the impregnated Pt NP was determined to be $\langle R_g \rangle_G = 1.03 \pm 0.01$ nm, which is about 22% higher than the corresponding value for Pt NPs in the colloidal suspension, $\langle R_g \rangle_G = 0.81 \pm 0.01$ nm.

2.2.4. Discussion of SAXS Results

The structural parameters derived from dry NPs (TEM), NPs embedded in ethanol and impregnated in the SBA-15 substrate (SAXS) are reported in **Table 1**. The 22% increase in the average gyration radius of the impregnated NP is remarkable and can only be understood by a change in the shape of the NP when passing from the colloidal solution into the nanopores of the SBA-15. This change in shape has also implications in the EXAFS results discussed below.

2.3. X-ray Absorption Spectroscopy

2.3.1. EXAFS

The same capped NPs in liquid suspension and impregnated in SBA-15 that were studied by SAXS were also investigated by EXAFS on the Pt L_3-edge. EXAFS provides the average coordination number and nearest neighbor distances of the Pt atoms. Bulk Pt was also used for comparison. All spectra were recorded at a temperature of 20 K to decrease the influence of thermal disorder. The results of a multiple scattering analysis[17] of the EXAFS data are reported in **Table 2** and **Table 3**. Details of the analysis and fitting of the spectra are shown in the SI.

The Fourier transform (FT) of the data corresponding to the NPs in suspension exhibits a clear decrease in amplitude with respect to bulk Pt, as shown in **Figure 3**. This is apparent in the peak amplitudes corresponding to first, second and third neighbor shells. These changes are a consequence of

Table 1. Size parameters corresponding to Pt NP in different environments. Errors for the last digit are in brackets. Units for R are nanometres.

TEM Dry NPs	SAXS NPs suspended in ethanol		SAXS Supported NPs
$\langle R \rangle$	$\langle R \rangle_G$	$\langle R_g \rangle_G$	$\langle R_g \rangle_G$
1.18 ($\sigma = 0.12$)	1.05(1)	0.81(1)	1.03(1)

NANO MICRO small

Table 2. Average coordination numbers N_i (i = shell index), and corresponding Pt–Pt distances obtained by multiple scattering analysis of EXAFS data for a suspension of PVP-capped Pt NPs in ethanol. Strictly N_i is the average degeneracy number, which coincides with the average coordination number for single scattering paths (as for all cases shown in this table). ΔE_0 is the Fermi Energy correction, σ^2 the variance of the Debye-Waller factor and $C_3$the value of the third cumulant in the EXAFS analysis. Errors for the last digit are in brackets. Although only single scattering paths are shown in the table, other fits were also performed using both single and multiple scattering paths.

Path	N_i	ΔE_0 [eV]	Distance [nm]	σ^2 [nm^2] $\times 10^{-6}$	C_3 [nm^3] $\times 10^{-7}$
1	9.3(5)	2.4(7)	0.276(1)	35(1)	–0.6(3)
2	4(1)	-	0.391(1)	39(9)	-
5	14(2)	-	0.480(1)	50(6)	-
8	6(1)	-	0.554(1)	53(7)	-
17	5(2)	-	0.616(2)	53(7)	-

Table 3. Average coordination numbers N_i and corresponding Pt–Pt distances obtained by multiple scattering analyses of EXAFS data for Pt NPs embedded in SBA-15. Only single scattering paths are shown in the table, but other fits were also performed using both single and multiple scattering paths.

Path	N_i	ΔE_0 [eV]	Distance [nm]	σ^2 [nm^2] $\times 10^{-6}$	C_3 [nm^3] $\times 10^{-7}$
1	7.2(7)	1(2)	0.274(1)	40(3)	–1.0(7)
2	4(2)	-	0.390(1)	60(25)	-
5	6(4)	-	0.480(1)	50(24)	-
8	4(2)	-	0.553(2)	61(21)	-
17	6(5)	-	0.616(3)	61(21)	-

the small size of the NPs, which results in a decrease in the average coordination number N relative to the bulk. Our EXAFS results indicate that the average number of first neighbor Pt atoms decreases from 12 for bulk Pt to 9.3 for the Pt NPs studied here (see Table 2).

As shown in Figure 3 the FT peaks from the NPs impregnated in SBA-15 exhibit an additional decrease compared to those of the NPs in solution. This additional decrease indicates a further decrease in first neighbor coordination number, from 9.3 to 7.2 (Table 2 and Table 3), which can be associated to changes in the local structure and/or shape of the NP when incorporated in the SBA-15 substrate. This structural change indicates a non-negligible interaction between the Pt NP with the SBA-15 substrate even in the presence of the PVP capping agent on the NPs.

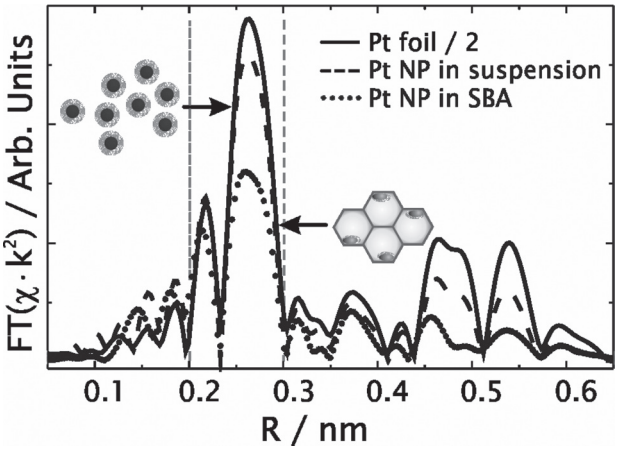

Figure 3. Fourier transform of EXAFS spectra acquired at 20 K for colloidal PVP-capped Pt NPs (dashed line), NPs embedded in SBA-15 (dotted line) and bulk Pt (metal foil, solid line).

Assuming that the Pt nanoparticles are spherical we can calculate the first-nearest-neighbor single-scattering average coordination number as a function of particle radius for closed-shell clusters by interpolating the plot for open-shell clusters.[18,19] In addition, the shape of the particles can also be inferred from the EXAFS if higher order coordination shells are considered. This is manifested by strong changes in the average coordination numbers of the shells as function of particle size for different shapes.[20,21] From the multiple scattering fits of the data obtained for colloidal NPs (see SI) we obtained average coordination numbers for the first three Pt shells that are compatible with a spherical particles with average radii between 0.8–1.05 nm, which is in good agreement with the average radius determined by TEM (1.18 nm ($\sigma = 0.12$)) and and SAXS (1.05 nm).

2.3.2. Nanoparticle Shape Modeling

In order to obtain a quantitative insight into the shape of the NPs impregnated in SBA-15 we model the NP as spherical caps (see inset of **Figure 4**) with a base radius, R_H, and height, H. With this simple model we can calculate the average coordination number for the first Pt–Pt shell as a function or R_H and H. A plot of the values obtained as a function of R_H is shown in Figure 4, restricting the calculation to NPs with the same number of atoms (approximately 200) as in the original colloidal NPs. H values shown in Figure 4 range from

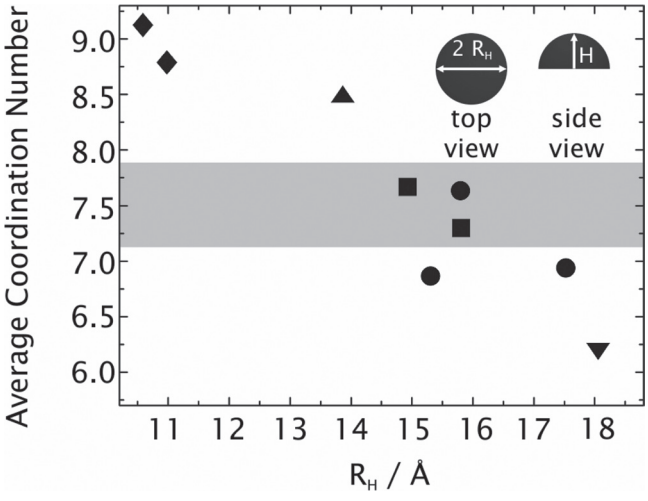

Figure 4. Average coordination number for the first coordination shell of Pt atoms in a NP with a spherical cap shape as a function of base radius R_H and height H (H values: ◆:0.98 nm, ▲: 0.78 nm, ■: 0.59 nm, ●: 0.39 nm, ▼: 0.19 nm). The gray region corresponds to NPs with the same average co-ordination number than the one obtained from the EXAFS analysis.

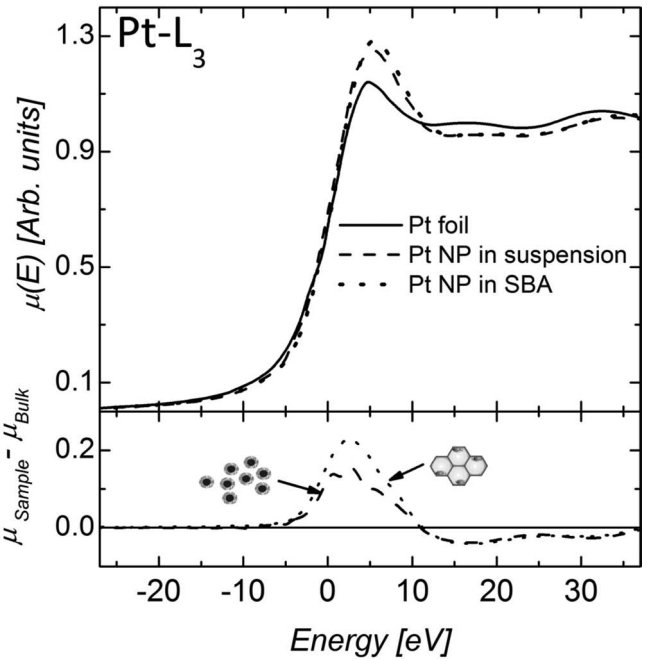

Figure 5. XANES spectrum at the Pt L_3-edge for Pt foil (black line) and for Pt NPs before (dashed line) and after (dotted line) impregnation in the SBA-15 substrate. The lower part of the figure shows the differences relative to the Pt foil. These difference are attributed to the change in the density of Pt *5d* holes in the NP relative to the Pt bulk.

0.2–1 nm. The shaded band corresponds to the average coordination number N obtained from the fit of the EXAFS data. The spherical caps in that region have base diameters $2R_H$ between 3.0 and 3.2 nm, which are substantially larger than the diameter of the Pt NPs in solution. Their height H varies between 0.39 and 0.59 nm, which corresponds to about two or three atomic monolayers.

2.3.3. XANES

The electronic state of the Pt atoms was studied by X-ray absorption near-edge structure (XANES) at the Pt L_3-edge before and after impregnation in the SBA-15. The results are shown in **Figure 5**. Transitions from the $2p_{3/2}$ core level to vacant *5d* states give rise to a resonance peak, commonly known as the white line (WL). The line shape contains information on the final state of the transition. Increases in the resonant peak intensity relative to the pure element reflect the number of d-electrons removed from the absorber due to chemical bonding.[22] Meitzner et al.[23] observed that the resonance was more intense for highly dispersed clusters than for the bulk metal.

As it can be seen in Figure 5 there is a change in the WL intensity between both the colloidal NPs and the NPs impregnated in SBA-15 relative to Pt bulk. The largest variation is observed for NPs in contact with the SBA-15 substrate. The variation of the WL intensity in different environments (liquid media and the SBA porous material) is indicative of a significant electronic interaction between the Pt NPs and the SBA support.

2.3.4. Discussion of EXAFS/XANES Results

The decrease in the average coordination number $N_1$for the capped Pt NPs impregnated in SBA-15 derived from EXAFS may be attributed to three different effects: i) the presence of a fraction of Pt atoms in small clusters or as individual ions interacting with the support atoms, ii) surface disorder in the small NP leading to a smaller N value while preserving the spherical shape of the particle,[24] and iii) an overall change in the shape of the Pt NP, as proposed in this work.

The first effect can be discarded because the presence of small clusters or individual Pt atoms should also occur in the NP in solution. The second effect can also be discarded because the decrease in the average coordination number after impregnation is around 22% and cannot be explained as a surface relaxation effect. The model proposed by Frenkel et al.[24] predicts a maximum decrease of about 10% in the average coordination factor due to this effect.

We therefore conclude that our proposed model of the change in NP shape is the most plausible. The model preserves the volume of the NP and increases the surface area, therefore decreasing the average coordination number of the Pt atoms. Similar to observations made in previous studies,[25–27] the EXAFS results indicate a contraction in the average first neighbor distance relative to bulk Pt. The fact that this contraction for NPs embedded in SBA-15 is higher than for NP in solution can be explained as a consequence of the larger amount of atoms at the surface of the flattened NP. An analogous effect for supported NPs was previously assigned to a charge transfer process from the environment to the NP surface.[28] The Debye-Waller variance (σ^2) and the third cumulant (C_3) also depend on the NP environment. According to the various literature reports[28,29] these variations could be assigned to modifications in the interatomic potential when either the size or the NP environment change. Additional EXAFS studies of the same system at different temperatures are needed in order to elucidate this issue.

3. Conclusion

The structure and shape of PVP-capped Pt NPs in a dry state, in ethanol, and embedded in SBA-15 mesoporous silica were characterized using TEM, SAXS, EXAFS, and XANES. We have clearly shown that the interaction between the Pt NPs and the SBA-15 substrate induces changes of the NP shape. The results derived from two independent techniques (SAXS and EXAFS) lead to the same conclusion concerning the shape changes of the Pt NPs. This agreement implies that the basic assumptions about the simple model proposed for the NP shape are reasonable.

Even if the absence of an important contribution from Pt bonds with oxygen from the substrate, probably due to the presence of the PVP-capping, an electronic interaction is evidenced by the occupancy variation at the 5d level. This result has important implications in the understanding of NP–substrate interactions and in applications such as catalysis. However, from the results of this work the role of the PVP capping on the interaction between the NPs and SBA

NANO MICRO small

surface was not clearly identified. Thus this emerges now as an interesting topic which requires further study to be clearly understood.

4. Experimental Section

Synthesis of Samples: The Pt NPs were prepared by reduction of hexachloroplatinic acid (H_2PtCl_6) in ethylene glycol in the presence 55 000 MW poly-*N*-vinylpyrollidone (PVP).[30,31] They were then precipitated by the addition of acetone and re-suspended in ethanol. This solution was used to impregnate the mesoporous SBA-15 silica. Mesoporous SBA-15 type silica was synthesized in our laboratory according to a method reported by the Stucky group.[32]

General Methods: Real space analysis was performed using a FEI Tecnai TEM on specimens prepared by depositing a dilute NP suspension onto a C/Formvar/Cu TEM grid. Reciprocal space information was obtained from SAXS experiments performed at the Laboratório Nacional de Luz Síncrotron (LNLS), in Campinas, Brazil. SAXS measurements were performed at the SAXS-1 beam line[33] using two types of samples: i) PVP-capped NPs in ethanol and ii) the same NPs embedded in a powdered SBA-15 substrate. The spectra were normalized to equivalent intensity of the direct X-ray beam. The isotropic SAXS intensity was measured as a function of the scattering vector $q = (4\pi/\lambda)\sin\theta$, λ being the wavelength (λ = 0.161 nm), and 2θ the scattering angle. The parasitic scattering from slits was subtracted. Because of the small cross-section of the direct X-ray beam at the detector plane the SAXS curve did not need to be corrected for smearing effects.

The EXAFS experiments at the Pt L_3 edge (11563.7 eV) were performed at the XAFS-1 beam-line at 20 K in transmission mode using gas ionization chambers as detectors. Homogeneous samples of NPs mounted on membranes were obtained by filtering the Pt NP suspensions in ethanol. The thickness of the membranes provided an X-ray absorption jump at the Pt L_3 edge of approximately 0.75.

Supporting Information

Supporting Information is available from the Wiley Online Library or from the author.

Acknowledgements

This work was partially supported by LNLS under D04B-XAFS1-7683 proposal, PIP 112-200801-03079 (CONICET, Argentina), PICT-2008-00038 (ANPCYT and CNPq collaborative project between Argentina and Brazil). MMK, GAS and MBS are supported by the Director, Office of Science, Office of Basic Energy Sciences, Chemical Sciences, Geosciences, and Biosciences Division, under the Department of Energy Contract No. DE-AC02-05CH11231.

[1] Y. Li, M. A. El-Sayed, *J. Phys. Chem. B* **2001**, *105*, 8938–8943.
[2] D. Meisel, W. A. Mulac, M. S. Matheson, *J. Phys. Chem.* **1981**, *85*, 179–187.
[3] R. Narayanan, M. A. El-Sayed, *Nano Lett.* **2004**, *4*, 1343–1348.
[4] I.-S. Park, K.-S. Lee, J.-H. Choi, H.-Y. Park, Y.-E. Sung, *J. Phys. Chem. C* **2007**, *111*, 19126–19133.
[5] X. H. Chen, M. Moskovits, *Nano Lett.* **2007**, *7*, 807–812.
[6] G. A. Somorjai, R. L. York, D. Butcher, J. Y. Park, *Phys. Chem. Chem. Phys.* **2007**, *9*, 3500.
[7] A. Miyazaki, I. Balint, Y. Nakano, *J. Nanoparticle Res.* **2003**, *5*, 69–80.
[8] H. Lee, S. E. Habas, S. Kweskin, D. Butcher, G. A. Somorjai, P. Yang, *Angew. Chem. Int. Ed.* **2006**, *45*, 7824–7828.
[9] B. H. Morrow, A. Striolo, *Nanotechnology* **2008**, *19*, 195711.
[10] A. Y. Stakheev, L. M. Kustov, *Appl. Catal. A: General* **1999**, *188*, 3–35.
[11] S. J. Tauster, S. C. Fung, R. T. K. Baker, J. A. Horsley, *Science* **1981**, *211*, 1121–1125.
[12] B. L. Mojet, J. T. Miller, D. E. Ramaker, D. C. Koningsberger, *J. Catalysis* **1999**, *186*, 373–386.
[13] R. Yu, H. Song, X.-F. Zhang, P. Yang, *J. Phys. Chem. B* **2011**, *109*, 6940–6943.
[14] J. K. Nørskov, T. Bligaard, J. Rossmeisl, C. H. Christensen, *Nat. Chem.* **2009**, *1*, 37–46.
[15] A. Guinier, *Small-Angle Scattering of X-rays.*, John Wiley & Sons Inc., New York **1955**.
[16] P. F. Fulvio, S. Pikus, M. Jaroniec, *J. Mater. Chem.* **2005**, *15*, 5049–5053.
[17] S. I. Zabinsky, J. J. Rehr, A. Ankudinov, R. C. Albers, M. J. Eller, *Phys. Rev. B* **1995**, *52*, 2995–3009.
[18] R. B. Greegor, F. W. Lytle, *J. Catalysis* **1980**, *63*, 476–486.
[19] J. M. Ramallo-López, F. G. Requejo, A. F. Craievich, J. Wei, M. Avalos-Borja, E. Iglesia, *J. Mol. Catalysis A: Chemical* **2005**, *228*, 299–307.
[20] A. Jentys, *Phys. Chem. Chem. Phys.* **1999**, *1*, 4059–4063.
[21] A. I. Frenkel, *J. Synch. Rad.* **1999**, *6*, 293–295.
[22] F. W. Lytle, P. S. P. Wei, R. B. Greegor, G. H. Via, J. H. Sinfelt, *J. Chem. Phys.* **1979**, *70*, 4849–4855.
[23] G. Meitzner, G. H. Via, F. W. Lytle, J. H. Sinfelt, *J. Phys. Chem.* **1992**, *96*, 4960–4964.
[24] A. Yevick, A. I. Frenkel, *Phys. Rev. B* **2010**, *81*, 115451.
[25] J. H. Kang, L. D. Menard, R. G. Nuzzo, A. I. Frenkel, *J. Am. Chem. Soc.* **2006**, *128*, 12068–12069.
[26] B. Roldan Cuenya, A. I. Frenkel, S. Mostafa, F. Behafarid, J. R. Croy, L. K. Ono, Q. Wang, *Phys. Rev. B—Condens. Mat. Mater. Phys.* **2010**, *82*.
[27] S. I. Sanchez, L. D. Menard, A. Bram, J. H. Kang, M. W. Small, R. G. Nuzzo, A. I. Frenkel, *J. Am. Chem. Soc.* **2009**, *131*, 7040–7054.
[28] A. I. Frenkel, C. W. Hills, R. G. Nuzzo, *J. Phys. Chem. B* **2001**, *105*, 12689–12703.
[29] L. J. Giovanetti, J. M. Ramallo-López, F. G. Requejo, D. I. Garcia-Gutierrez, M. Jose-Yacaman, A. F. Craievich, *J. Phys. Chem. C* **2007**, *111*, 7599–7604.
[30] R. M. Rioux, H. Song, J. D. Hoefelmeyer, P. Yang, G. A. Somorjai, *J. Phys. Chem. B* **2005**, *109*, 2192–2202.
[31] H. Song, R. M. Rioux, J. D. Hoefelmeyer, R. Komor, K. Niesz, M. Grass, P. Yang, G. A. Somorjai, *J. Am. Chem. Soc.* **2006**, *128*, 3027–3037.
[32] D. Zhao, Q. Huo, J. Feng, B. F. Chmelka, G. D. Stucky, *J. Am. Chem. Soc.* **1998**, *120*, 6024–6036.
[33] G. Kellermann, F. Vicentin, E. Tamura, M. Rocha, H. Tolentino, A. Barbosa, A. Craievich, I. Torriani, *J. Appl. Crystallogr.* **1997**, *30*, 880–883.

Received: June 28, 2011
Published online: December 23, 2011

